Proceedings of ASME Turbo Expo 2011
GT2011
June 6-10, 2011, Vancouver, British Columbia, Canada

GT2011-46048

EXPERIMENTAL ANALYSIS OF THE DYNAMIC CHARACTERISTICS OF A HYBRID AEROSTATIC BEARING

Laurent RUDLOFF(1), Mihai ARGHIR(1), Olivier BONNEAU(1), Sebastien GUINGO(2), Guillaume CHEMLA(2), Emelyne RENARD(3)
(1) Institut PPRIME, CNRS UPR3346, Université de Poitiers
(2) SNECMA Space Engine Division, Vernon
(3) Centre National d'Etudes Spatiales, Evry
FRANCE

ABSTRACT
The dynamic characteristics of a hybrid aerostatic bearing are experimentally investigated on a test rig consisting of a rigid rotor driven by an impulse turbine located at its midlength. The rotor is horizontally mounted and is supported by two identical aerostatic bearings at its ends. Both the impulse turbine and the aerostatic hybrid bearings are fed with air. The actually available resources enable to attain feeding pressures up to 5 bar in the bearings and rotation speeds up to 60 krpm. Under these conditions the dynamic load on the rotor is much larger than the static load engendered by its weight. Dynamic loads consist either of impacts provided by a hammer or of added unbalance masses. The test rig can measure the bearing feeding pressures, the rotation speed, the impact force, the displacements of the two bearings and the bearing housing accelerations. This experimental information together with the equations of motion of the rotor enables the identification of the dynamic coefficients of the bearings. A second identification procedure using the same impact hammer is enabled by the fact force transducers are mounted between the bearing housing and its support. The dynamic coefficients of the bearings can then be obtained from the equation of motion of its housing.
Unbalance response provide a convenient way for verifying the accuracy of the identified dynamic coefficients. Therefore these coefficients are injected in the equations of motion of a four degrees of freedom rigid rotor and the theoretical results are compared with values measured on the test rig. Comparisons show that predictions are acceptable but become less accurate at high rotation speeds where large dynamic forces are needed for exciting the corresponding synchronous frequencies.

INTRODUCTION
Aerostatic bearings are well known components that entered in use almost fifty years ago. Many textbooks tackle this subject in a more or less extensive manner [1-4]. These bearings are used when needing high precision, very high rotation speed and good stiffness and when a source of compressed air is easily available. The main applications are small turbomachinery lubricated with the process fluid or air spindles for the machining industry. In these applications they are intended to replace ball or roller bearings that have limited life duration; when subject to wear ball or roller bearing generate high supersynchronous vibrations that affect precision and consume more power. Hybrid aerostatic bearings don't suffer from these drawbacks and have a theoretically infinite life duration that is affected only by start and stop phases. However they are not products on the shelf and each new bearing necessitates a dedicated design. This aspect is enforced by the fact that contrary to ball or roller bearings, hybrid aerostatic bearings are prone to self induced vibrations ("pneumatic hammer" and "oil whirl"). These instabilities are discussed in the above cited textbooks and are of paramount importance because, once entering these regimes, the aerostatic bearing has no possibility of generating supplementary damping and will generally lead to contact. Theoretical prediction methods are therefore of paramount importance. There is a very large amount of work tackling the theoretical analysis of aerostatic bearings. Most of them are based on Reynolds equation, other few on the "bulk flow" system of equations. All these methods have an acute need of experimental validations because the theoretical analysis of aerostatic bearings must take into account the presence of restrictors (orifices, capillary, slits, etc.) or film discontinuities that cannot be dealt with in the simplifying frame of Reynolds or "bulk flow" equations. Experimental validations have then a similar importance to theoretical prediction methods.
The most recent and complete work dealing with the experimental analysis of aerostatic bearings are those of San Andres et al. [5-9] and of the research team at Politecnico di Torino [10-12]. The experimental results of San Andres and co-

workers were obtained on a test rig consisting of a light rotor supported by two identical bearings. The rotor incorporates an electric motor at its midlength and excitation is provided by adjusting unbalance loads. Many types of air pressurized bearings (lobed, tilting pad) were tested targeting turbomachinery applications. The careful system for aligning the bearings shows that the test rig is mainly focused on testing bearings and not modeling a rotating machine.
The work performed at Politecnico di Torino has many facets that are well revised in reference [12]. The test rigs consist of rigid rotors supported by air pressurized journal and thrust bearings and driven by impulse turbines. The journal and the thrust bearings are rigidly mounted as on most rotating machines. The test rigs then models spindles used in the machining industry.

The present work is part of a collaborative research and development project carried on with *Snecma Space Engine Division* and *Centre National d'Etudes Spatiales*. Its purpose is to introduce a test rig based on a rigid rotor supported by two identical bearings. The intent of the test rig is to enable measurements of dynamic coefficients of the bearings that will either validate theoretical models or characterize new designs.

NOMENCLATURE

A	acceleration FFT component [m/s^2]
$A^{(0)}$, $A^{(1)}$, $B^{(0)}$,	coefficients defined by eq. (21)
C	damping [Ns/m]
f	force [N]
$[G]$	gyroscopic matrix
J_t, J_p	transverse and polar moment of inertia [kg·m^2]
K	stiffness [N/m]
l	length [m]
M	rotor mass [kg]
M_b	mass of the instrumented bearing [kg]
m	moment [Nm]
$[P]$	matrix defined by eq. (16)
$\{q\}$	variables vector
t	time [s]
u	unbalance [kg·m]
x, y	coordinate and distances [m]
Z	bearing impedance
Ω	rotation speed [rad/s]
ω	excitation speed [rad/s]
θ, Φ	rotation angle [rad]
Subscripts	
$1, 2$	first, second bearing
a	absolute reference frame
b	unbalance
h	bearing housing
imp	impact
$\Re, \Im$	real, imaginary part

DESCRIPTION OF THE TEST RIG

The test rig shown in Fig. 1 consists of a horizontal hollow rotor supported by two identical aerostatic hybrid bearings and driven by a double impulse (Pelton) turbine. The turbine is machined directly onto the rotor surface and is located at its midlength. The Pelton turbine is supposed to drive the shaft with no axial loads. However, pressurized air injectors are axially mounted at the both extremities of the rotor. The two impinging air jets will eliminate any axial displacement with minimum friction and without interfering with the radial displacement of the rotor. Additional unbalance masses can be mounted at the extremities of the rotor.
This rotor is supported by two identical aerostatic bearings of 45 mm diameter and 50 µm radial clearance located at its extremities. The design of the bearings was made having in mind that pneumatic hammer instability is the major risk. This self induced vibration is favored by two parameters [4]: the depth of the recesses and the pressure ratio P_r/P_s. Usual practice for air bearings is to avoid any recess and to ensure a large P_r/P_s ratio. For example ratios close to 0.7 ensure a maximum direct stiffness but with the risk of pneumatic hammer instability. Larger values will avoid this risk [4]. The bearing was then designed with rectangular shallow recesses of 200 µm depth, 15 mm radial length, 20 mm axial length and with orifice restrictors of 2 mm diameter. This large diameter of the orifice leads to pressure ratios close to 0.9.
The bearings are mounted on pedestals that can be independently aligned. Pedestals are considered as being rigid because their first proper mode is above 1.2 kHz, i.e. 40% higher that the maximum envisaged rotation speed. They are also made of stainless steel in order to avoid any oxidation that might create difficulties in aligning the two pedestals. The pedestals are provided with positioning systems enabling two translations and two rotations. A distinct system enables the rigid fixation of the two pedestals once the bearings are aligned. This way positioning and maintaining the bearings are two uncoupled functions. A special rotor is used for aligning the bearings. Four inductive displacement probes are placed on each bearing housing and are mounted two by two in the front and rear axial planes of bearing.

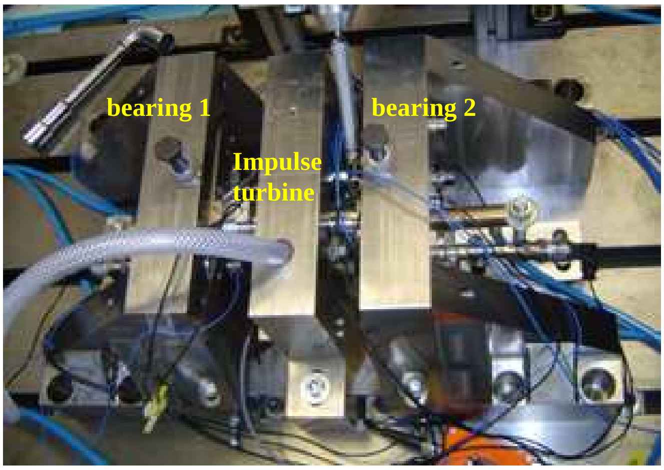

Figure 1: Cut view of the test rig.

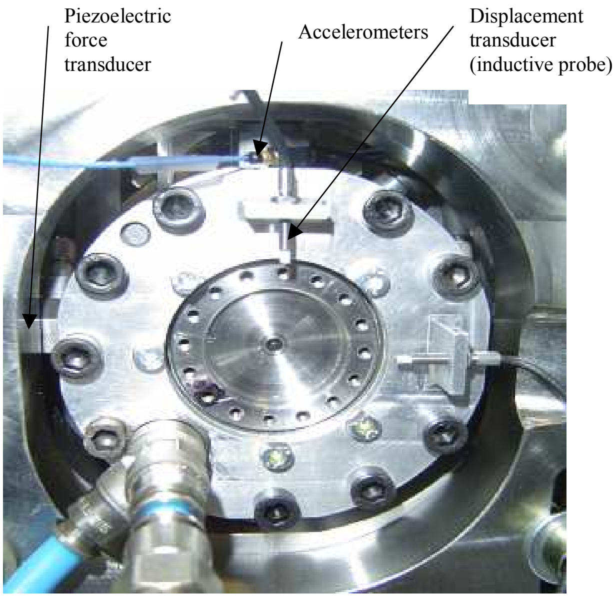

Figure 2 : Aerostatic bearing and instrumentation.

The special rotor and the eight displacement probes enable the measurement of the clearance and of the misalignment in each bearing and between the bearings. The alignment of the bearings is made by mounting the special rotor and by matching the metrological radial clearance as close as possible. During the mounting of the special rotor the bearings are pressurized in order to minimize the possibility of hazardous contact. The air pressurization is then cut-off and the radial clearance in the bearings is measured by manually pulling the shaft and by measuring the maximum and minimum displacements. The alignment process is terminated when the measured clearances in the two bearings are as close as possible to the metrological ones. The pedestals are then rigidly fixed on the table. The remaining differences between the radial clearance of the pedestal mounted bearings and the metrological measured one is the limit of the alignment procedure.

Each bearing is mounted on the pedestal via four piezoelectric force transducers (Fig.2). They enable the measurement of the force transmitted from the bearings to the rigidly fixed pedestals. Due to this relatively flexible mounting, two accelerometers are placed on each bearing in two orthogonal directions. The instrumentation of the bearings is completed by two pressure gauges and by two regulation valves that enable the adjustment of the supply pressure independently for each bearing.

External excitations are imposed by using an electric impact hammer rigidly mounted on the table. The impact force is measured by a piezoelectric transducer mounted between a stinger and the hammer head. The force is controlled by adjusting a potentiometer. The original impact head was replaced by a small ball bearing for limiting interferences with the rotating impact (shaft) surfaces, a solution borrowed from reference [13]. The original stinger of the impact hammer was also replaced by a longer one. These modifications required a slight recalibration of the force.

The impulse (Pelton) turbine is fed by a specific distributor. The position of the distributor relative to the rotor is also adjusted after aligning the pedestals but this tuning is less sensitive and can be made by using some static contact displacement measuring devices. A pneumatic servo valve controls the pressure of the air feeding the distributor and the resulting velocity of the rotor.

All the instrumentation used on the test rig indicated in Table 1 and is schematically depicted in Fig. 3. The displacements probes used for aligning the bearings are also used for measuring dynamic displacements. All measured signals are saved on a computer before post-treatment.

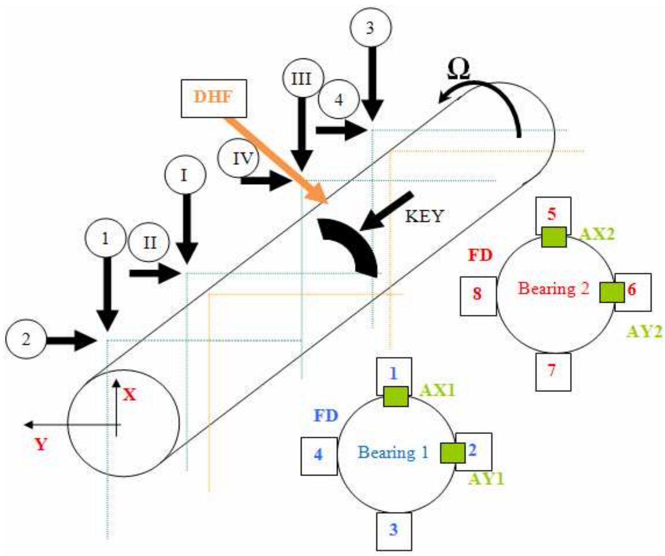

Figure 3: Test rig instrumentation

Table 1. Test rig instrumentation (see Fig. 3)

Name	Probe type	Measure
I, II, III, IV	Inductive probe	Shaft displacement
1, 2, 3, 4	Inductive probe	Displacements used for alignment
1, 2, 3, 4	Piezoelectric force transducer	Force between bearing 1 and pedestals
5, 6, 7, 8	Piezoelectric force transducer	Force between bearing 2 and pedestals
KEY	Optic transducer	Rotation frequency
DHF	Piezoelectric impact transducer	Hammer Impact Forces
AX1, AY1	Accelerometer	Acceleration bearing 1
AX2 , AY2	Accelerometer	Acceleration bearing 2

DYNAMIC MEASUREMENTS

Two types of dynamics measurements were made. The first tests were performed by using the external excitation provided by the impact hammer and their goal was the measurement of the rotordynamic coefficients of the bearings. The second tests were made by adding measured unbalance masses and were intended to verify the accuracy of the measured dynamic coefficients.

Mathematical model

The test rig and its instrumentation enable the measurement of dynamic coefficients by using two different identification methods.

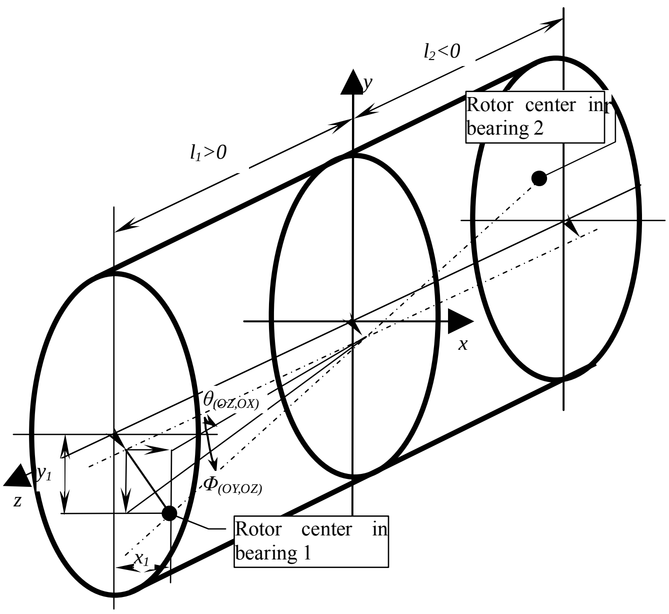

Figure 4: Coordinate system

Identification method 1. Rotor eq. of motion

The first method is based on the developments performed by DeSantiago [13] for a rigid rotor supported on two bearings. The equations of motion of the rigid rotor are (Fig. 4).

$$[M]\{\ddot{q}_a\}=\{f\}+\{f_b\}-\Omega[G]\{\dot{q}_a\} \quad (1)$$

$$\{q_a\}=\{x_a \quad y_a \quad \theta_a \quad \Phi_a\}^T \quad (2)$$

where x_a, y_a, θ_a and Φ_a are the displacements and the rotations of the centre of mass in an absolute reference frame. The vectors $\{f\}$ and $\{f_b\}$ represent the external forces and the forces in the bearings. The last term stands for the gyroscopic effects. For a symmetric rotor, $l_1 = l > 0$ and $l_2 = -l < 0$ resulting :

$$x_a = (x_{a1} + x_{a2})/2\,,\ y_a = (y_{a1} + y_{a2})/2 \quad (3)$$

$$\theta_a = (x_{a1} - x_{a2})/2l\,,\ \Phi_a = -(y_{a1} - y_{a2})/2l \quad (4)$$

The equations of motions are then recast:

$$[M]\{\ddot{\tilde{q}}_a\}=\{f\}+\{f_b\}-\Omega[G]\{\dot{\tilde{q}}_a\} \quad (5)$$

$$\{\tilde{q}_a\}=\{x_{a1} \quad y_{a1} \quad x_{a2} \quad y_{a2}\}^T \quad (6)$$

$$[\tilde{M}]=\begin{bmatrix} M/2 & 0 & M/2 & 0 \\ 0 & M/2 & 0 & M/2 \\ J_t/2l & 0 & -J_t/2l & 0 \\ 0 & -J_t/2l & 0 & 0 \end{bmatrix} \quad (7)$$

$$[\tilde{G}]=\begin{bmatrix} 0 & 0 & 0 & 0 \\ 0 & 0 & 0 & 0 \\ 0 & -J_p/2l & 0 & J_p/2l \\ -J_p/2l & 0 & J_p/2l & 0 \end{bmatrix} \quad (8)$$

$$\{f(t)\}=\begin{Bmatrix} f_x(t) \\ f_y(t) \\ m_y(t) \\ m_x(t) \end{Bmatrix}=\begin{Bmatrix} f_{imp_x}+\sum u_b\Omega^2\cos(\Omega t) \\ f_{imp_y}+\sum u_b\Omega^2\sin(\Omega t) \\ f_{imp_x}l_{imp}+\sum (ul)_b\Omega^2\cos(\Omega t) \\ -f_{imp_y}l_{imp}-\sum (ul)_b\Omega^2\sin(\Omega t) \end{Bmatrix} \quad (9)$$

where f_{imp} represents the impact force, l_{imp} is its axial location, u_b is the unbalance and l_b is its axial location.
The forces in the bearings are expressed using the stiffness and damping coefficients.

$$\{f_b\}=-[\tilde{K}]\{\tilde{q}\}-[\tilde{C}]\{\dot{\tilde{q}}\} \quad (10)$$

$$[\tilde{K}]=\begin{bmatrix} K_{xx1} & K_{xy_1} & K_{xx2} & K_{xy_2} \\ K_{yx_1} & K_{yy_1} & K_{yx_2} & K_{yy_2} \\ K_{xx1}l & K_{xy_1}l & -K_{xx2}l & -K_{xy_2}l \\ -K_{yx_1}l & -K_{yy_1}l & K_{yx_2}l & K_{yy_2}l \end{bmatrix} \quad (11)$$

$$[\tilde{C}]=\begin{bmatrix} C_{xx1} & C_{xy_1} & C_{xx2} & C_{xy_2} \\ C_{yx_1} & C_{yy_1} & C_{yx_2} & C_{yy_2} \\ C_{xx1}l & C_{xy_1}l & -C_{xx2}l & -C_{xy_2}l \\ -C_{yx_1}l & -C_{yy_1}l & C_{yx_2}l & C_{yy_2}l \end{bmatrix} \quad (12)$$

where $\{\tilde{q}\}=\{x_1 \quad y_1 \quad x_2 \quad y_2\}^T$ are the relative displacements in the bearings measured by the proximity probes mounted on the bearing housing. The relation between $\{\tilde{q}_a\}$ and $\{\tilde{q}\}$ is:

$$\{\tilde{q}_a\}=\{\tilde{q}_h\}+\{\tilde{q}\} \quad (13)$$

where $\{\tilde{q}_h\}$ contains the displacements of the bearing housing.
Equations (10) and (13) are injected in the equation of motion (5).

$$[\tilde{M}]\{\ddot{\tilde{q}}\}+[\tilde{C}]\{\dot{\tilde{q}}\}+[\tilde{K}]\{\tilde{q}\}=\{f\}-\Omega[\tilde{G}]\{\dot{\tilde{q}}+\dot{\tilde{q}}_h\}-[\tilde{M}]\{\ddot{\tilde{q}}_h\} \quad (14)$$

where $\{\ddot{q}_h\}$ represent the acceleration of the bearing housing measured by the accelerometers and $\{\dot{q}_h\}$ are the corresponding velocities. After applying the Fourier transform, the equations of motion in the frequency domain yield :[1]

$$[\tilde{Z}]_i\{Q\}_i = \overbrace{\{F\}_i + \left(\omega_i^2[\tilde{M}] - j\omega_i\Omega[\tilde{G}]\right)\{Q\}_i - \left([\tilde{M}] - \frac{\Omega}{j\omega_i}[\tilde{G}]\right)\{A\}_i}^{RHS} \tag{15}$$

$$\{Q\}_i = \{X_1 \quad Y_1 \quad X_2 \quad Y_2\}_i^T \tag{16}$$

$$\{A\}_i = \{A_{X1} \quad A_{Y1} \quad A_{X2} \quad A_{Y2}\}_i^T \tag{17}$$

$$\{F\}_i = \{F_x \quad F_y \quad l_3F_x \quad -l_3F_y\}_i^T \tag{18}$$

where $[\tilde{Z}]_i$ is the bearing impedance matrix:

$$Z_{\alpha\beta_{1,2}} = K_{\alpha\beta_{1,2}} + j\omega C_{\alpha\beta_{1,2}},\ \alpha,\beta = x,y,\ j = \sqrt{-1} \tag{19}$$

The left hand side of the frequency domain equation is further simplified by taking into account that the bearings are identical (same geometry and same feeding pressure) $Z_{\alpha\beta\,1} = Z_{\alpha\beta\,2} = Z_{\alpha\beta}$ and by considering that both bearings are very close to centered working conditions so $Z_{xx} = Z_{yy}$ and $Z_{xy} = -Z_{yx}$. This is a plausible assumption for aerostatic bearings working with relative eccentricities lower than 40%. The left hand side of eq (15) then yields:

$$[\tilde{Z}]_i\{Q\}_i = \underbrace{\begin{bmatrix} X_1 + X_2 & Y_1 + Y_2 \\ Y_1 + Y_2 & -(X_1 + X_2) \\ l(X_1 - X_2) & l(Y_1 - Y_2) \\ -l(Y_1 - Y_2) & l(X_1 - X_2) \end{bmatrix}_i}_{[P]_i} \begin{Bmatrix} Z_{xx} \\ Z_{xy} \end{Bmatrix}_i \tag{20}$$

The bearing impedances are calculated in least square sense:

$$\begin{Bmatrix} Z_{XX} \\ Z_{XY} \end{Bmatrix}_i = \left([P]_i^T[P]_i\right)^{-1}[P]_i^T\,RHS \tag{21}$$

The resolution raises no problems because $rank[P]_i = 2$ and

$$-\left(X_{1i} + X_{2i}\right)^2 - \left(Y_{1i} + Y_{2i}\right)^2 \neq 0 \tag{22}$$

The impedances are averaged over n measurements.

$$\bar{Z}_{\alpha\beta\,i} = \frac{1}{n}\sum_{l=1}^{n} Z_{\alpha\beta\,il} \tag{23}$$

[1] Capital letter indicate the Fourier transform, $X_1 = FFT(x_1)$, etc.

and the dynamic coefficients are finally obtained from:

$$K_{\alpha\beta\,i} = \Re\left(\bar{Z}_{\alpha\beta\,i}\right),\ C_{\alpha\beta\,i} = \Im\left(\bar{Z}_{\alpha\beta\,i}\right)/\omega_i \tag{24}$$

It is to be underlined that the coordinates used for calculations correspond to the bearing mid planes. Corrections from the proximity probes to the bearings mid-planes were systematically performed.

Identification method 2. Bearing eq. of motion

The second method used for identifying the dynamic coefficients is based on the equations of motion of each bearing. This method is enabled by the fact that the bearings are mounted on the pedestals with piezoelectric force transducers and are also equipped with accelerometers. The excitation is still provided by the hammer impact but the piezoelectric transducers measure the force transmitted by the bearing to the pedestal. Displacements of the rotor relative to the bearing are measured by the formerly presented inductive transducers. This model is very similar to models already in use [14].

The equations of motion of each bearing written after applying the FFT are:

$$M_b\begin{Bmatrix} A_x \\ A_y \end{Bmatrix}_i + \begin{bmatrix} Z_{xx} & Z_{xy} \\ Z_{yx} & Z_{yy} \end{bmatrix}_i \begin{Bmatrix} X \\ Y \end{Bmatrix}_i = \begin{Bmatrix} F_x \\ F_y \end{Bmatrix}_i \tag{25}$$

With the same simplifying assumptions, $Z_{xx} = Z_{yy}$ and $Z_{xy} = -Z_{yx}$ this yields:

$$\begin{Bmatrix} Z_{xx} \\ Z_{xy} \end{Bmatrix}_i = \frac{1}{\left(X^2 + Y^2\right)_i}\begin{bmatrix} X & Y \\ Y & -X \end{bmatrix}_i\left(\begin{Bmatrix} F_x \\ F_y \end{Bmatrix}_i - M_b\begin{Bmatrix} A_x \\ A_y \end{Bmatrix}_i\right) \tag{26}$$

This equation must be separately applied for each bearing because the impact force is not in the middle of the rotor (the midlength of the rotor is occupied by the Pelton turbine) and so displacements in the two bearings are not identical. Dynamic coefficients are then identified by using either eq. (20) or (26).

Measurement methodology

Tests were made for three supply pressures, 3, 4 and 5 bars and for rotation speeds ranging from 0 to 50 krpm. It is known that dynamic coefficients of hybrid aerostatic bearings depend not only on the supply pressure and on the rotation speed but also on the excitation frequency. The impact force of the hammer excites a large spectrum of frequencies because its FFT a *sinc* function whose first zero frequency is around 2.5 kHz. However, due to low signal to noise ratio, the identification method is possible only in a limited bandwidth. Figure 5 depicts the spectrum of the impact force and of the displacement measured in a bearing. It can be seen that displacements are significant only in a bandwidth around 500

Hz. Increasing the impact force would excite higher frequencies but would also produce an overshoot of the bearing displacement that must remain lower than 10…20% of the radial clearance.

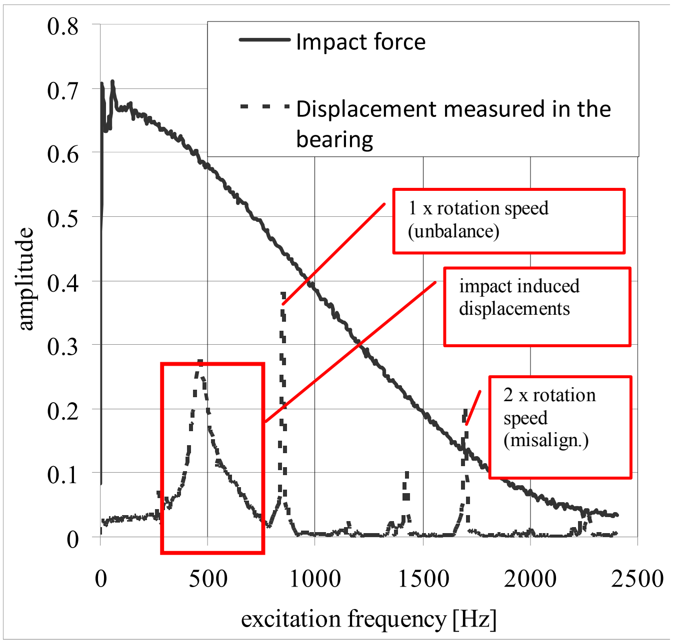

Figure 5: Spectrum of the impact force and of the displacement measured in the bearing. (P_s=5 bar, Ω=50 krpm).

The data acquisition time is relatively long (1s) with a sampling frequency of 2^{15} for easily catching the impact. The signal is then windowed and only 0.125 s from the impact are used for identifying the dynamic coefficients. A proper impact must not be located too close to the beginning or to the end of the data acquisition period. The impact force must be triggered for each working conditions because the stiffness of the bearing varies and for avoiding too low or too high dynamic displacements. Dynamic displacements after impact of 10µm for 3 bars, 8µm for 5 bars and 6µm for 4bars were generated in this chronological order. These values were imposed by the progressive wear of the hammer head (ball bearing) that progressively increased the risk of double impacts. In fact each test was repeated 12 times before averaging the dynamic coefficients but the number of impacts was much larger due to the above mentioned reasons (triggering the dynamic force, proper position of the impact inside the 1s acquisition period, etc.).

The signal of the accelerometers proved to be very noisy and difficult to use. An alternate way for deducing the same information was suggested by Murphy and Wagner [15]. The accelerations of the bearing housing are estimated from the forces measured by the piezoelectric transducers:

$$a_{x,y} = \frac{d^2\left(f_{x,y}/K_b\right)}{dt^2} \text{ or } A_{x,y_i} = -\omega_i^2 F_{x,y_i}/K_b \quad (27)$$

where K_b is the stiffness of the bearing housing mounted on piezoelectric force transducers. Each direction uses two force transducers of K_f=1.05·10^3 kN/µm each (manufacturer's data) so $K_b \approx 2K_f$.

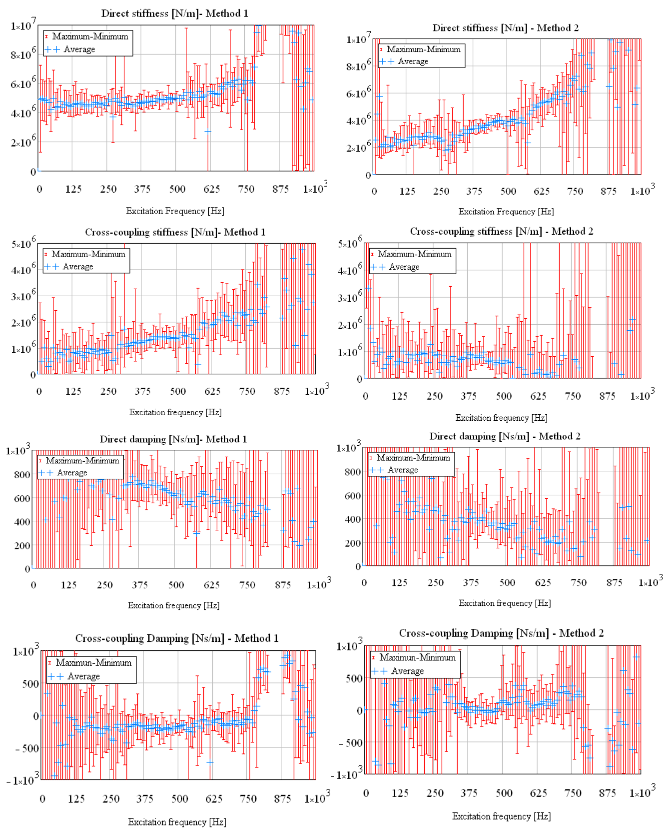

Figure 6: Dynamic coefficients identified from eq. 21 (Method 1) and from eq. 26 (Method 2) versus excitation frequency (P_s=5 bar, Ω=50 krpm)

RESULTS

Typical results stemming from identification method 1 (eq. 21) and method 2 (eq. 26) are depicted in Fig. 6. A rapid conclusion stemming from both dynamic models would be that K_{xx} increases with the excitation frequency while C_{xx} decreases. In fact, the results show that only a relatively narrow bandwidth of excitation frequencies located around 450 Hz can be used for identification, the rest of the results (especially those at high excitation frequencies) are very much affected by noise. Nevertheless, results stemming from the first identification

method have lower noise than the ones obtained from the second method. For the rest of working conditions the bandwidth where identification is possible is slightly changing but the results are qualitatively of the same order.
The variation of the dynamic coefficients for P_s=5 bar with the rotation speed is depicted in Fig. 6. The results are obtained by averaging the dynamic coefficients depicted in Fig. 5 over the small bandwidth of excitation frequency where the noise to signal ratio for the direct stiffness $K_{xx}=K_{yy}$ is less than 10%. This approximation leads to quasi-constant values of the dynamic coefficients with the excitation frequency. For the identification method 2, "b1" indicates the bearing close to the impact hammer were dynamic displacements are larger. The direct stiffness is almost constant with the rotation speed while the direct damping shows a light increase. The cross coupling stiffness increases almost linearly. All these tendencies are theoretically correct but the fact that the extrapolated K_{xy} shows a non-zero value for Ω=0 and the cross coupling damping is non-zero indicate that the experimental results are affected by errors.
Figure 6 shows also that the results stemming from method 1 lie between those obtained from method 2 and therefore seem to be more confident. One of the explanations would be the lack of accuracy in measuring accelerations and the ad-hoc solution provided by piezoelectric force transducers and eq. (27). The acceleration measurements required by method 1 intervene more as a correction to the RHS of eq. (21) for taking into account the movement of the bearing housing while they are an essential piece of information for method 2 and eq. 26. Results obtained for feeding pressures of 3 bar and 4 bar show the same behavior.
The dynamic coefficients stemming from method 1 and obtained with different feeding pressures are depicted in Fig. 8 versus the rotation speed. Previous conclusions stemming from Fig. 7 hold also for the results obtained for 3 bar and 4 bar: the direct stiffness is almost constant, the direct damping increases slightly and the cross-coupling stiffness increases almost linearly with rotation speed. Again, the non-zero values of the cross coupling damping may be considered as a warning of the measurement errors. The increase of the absolute value of the cross-coupling damping shows that measurements are less accurate with augmenting the rotation speed.

Unbalance response

Unbalance measurements were performed in order to test the accuracy of identified dynamic coefficients depicted in Fig. 8. An unbalance mass was added at one end of the rotor for exciting both the cylindrical and the conical rigid modes. Theoretical results were obtained by solving the equations of motion of the rotor given by eq. (14). The complementary information on acceleration housing was estimated using eq. (27).
The test matrix consisted of the same working conditions, i.e. P_s=3, 4 and 5 bar and Ω=0…50 krpm. The experimental and the theoretical results are presented in Fig. 9 for P_s=5 bar. Similar results were obtained for P_s=3 and 4 bar. The results

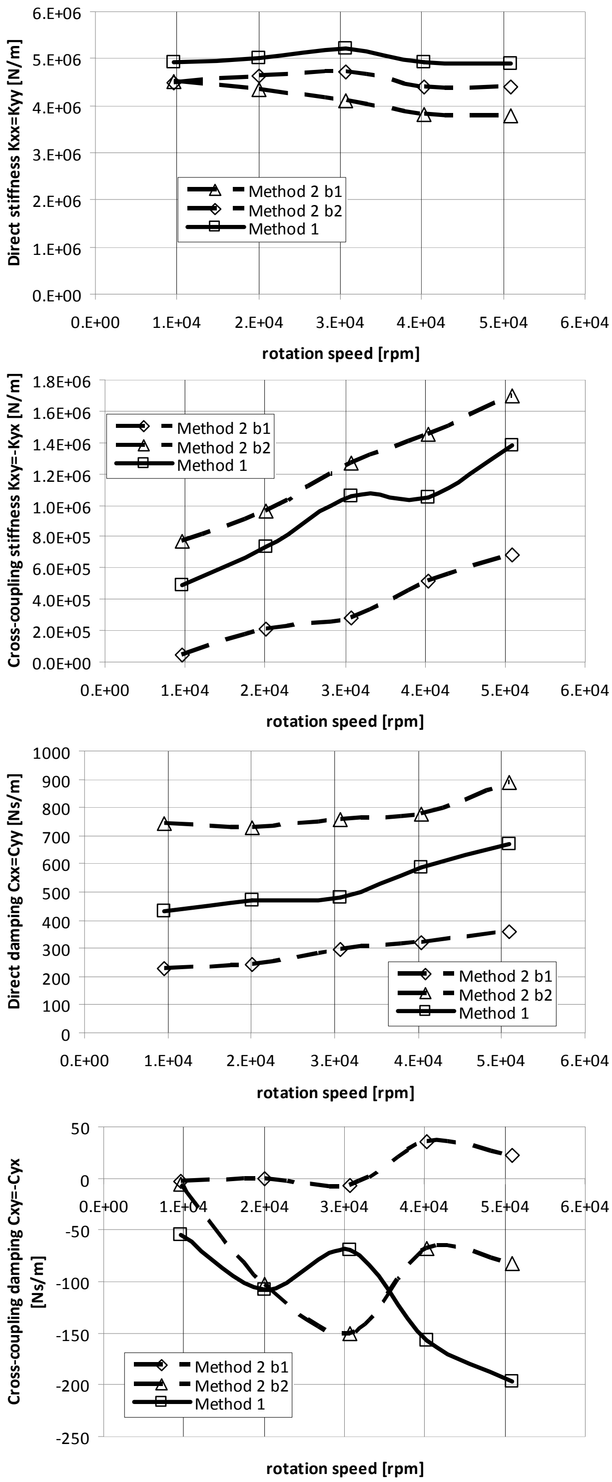

Figure7: Dynamic coefficients identified from eq. 21 (Method 1) and from eq. 24 (Method 2) versus rotation speed (P_s=5 bars)

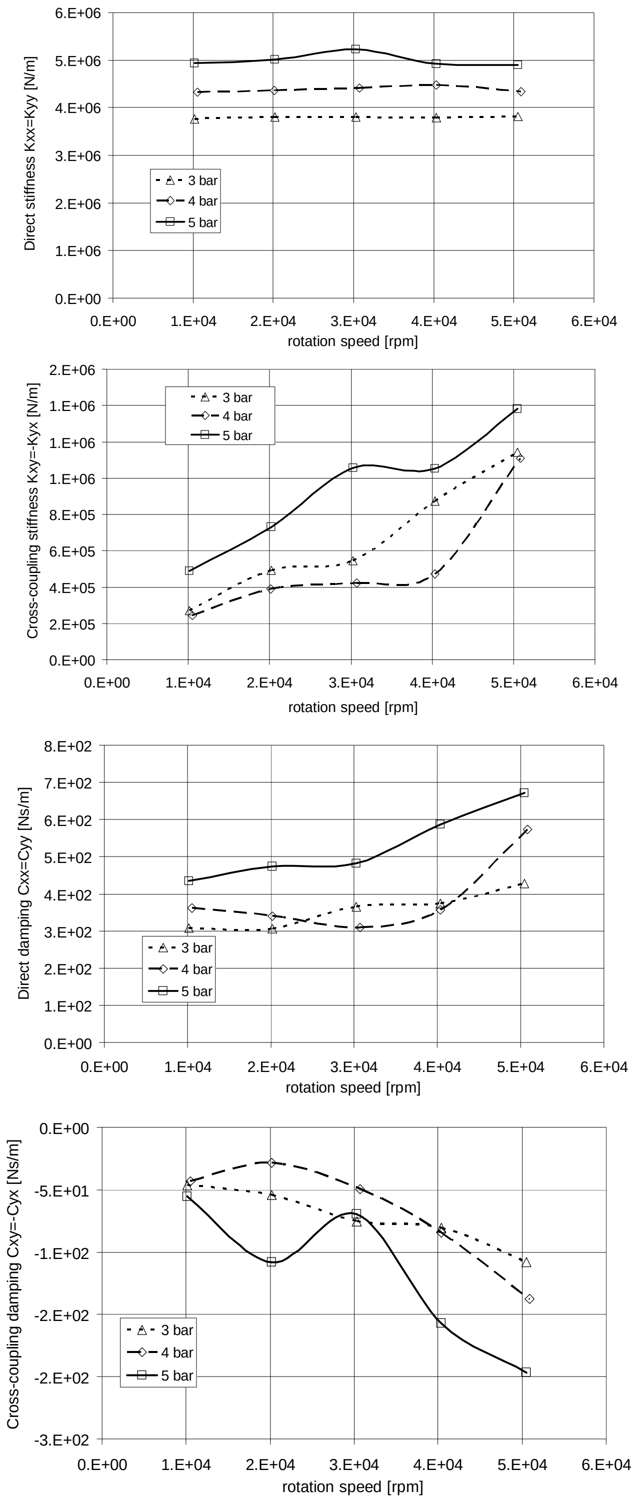

Figure8: Dynamic coefficients identified from Method 1 (eq. 21)

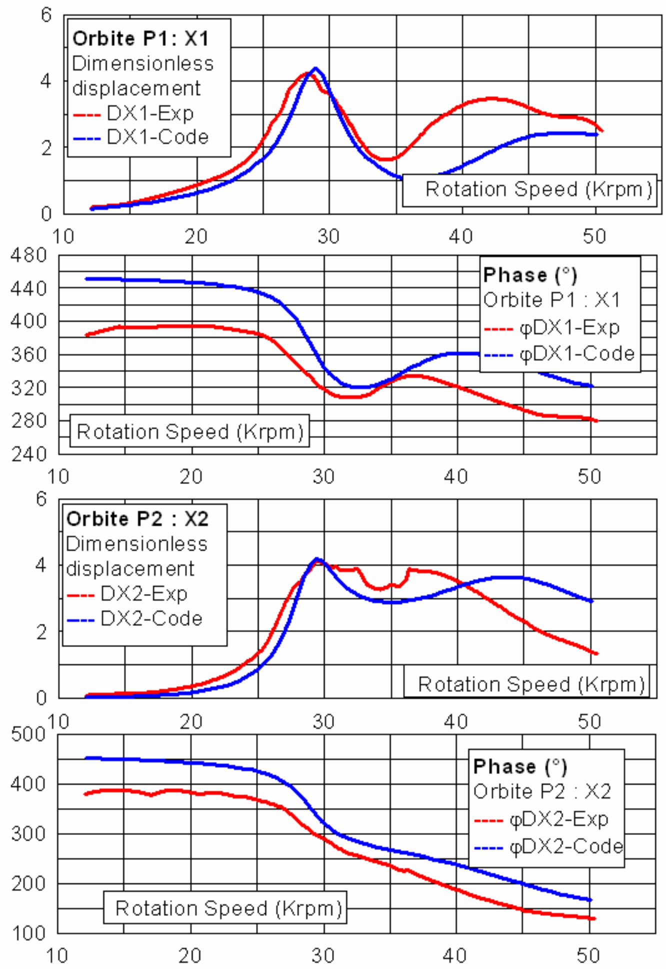

Figure 9 : Comparison of unbalance response, P_s=5 bar.

depict the x displacement amplitude for both bearings. The residual unbalance and the runout response of the rotor were extracted from the experimental data. The comparisons show that the cylindrical and conical modes of the rigid rotor are correctly predicted in terms of frequency thus indicating good experimental prediction of K_{xx}. The amplitudes of the measured unbalance response are slightly higher than the theoretical ones and show that the identified effective damping, $C_{eff}=C_{xx}-K_{xy}/\Omega$ is somewhat overestimated. Nevertheless the experimental and the theoretical responses show overall good agreement both in terms of amplitude and phase. These comparisons indicate that the identified dynamic coefficients depicted in Fig. 8 can be used for validating codes used for predicting the characteristics of hybrid aerostatic bearings.

SUMMARY, CONCLUSIONS AND PERSPECTIVES

The presented test rig and the identification methods are able to predict rotordynamic coefficients of hybrid aerostatic bearings in a limited bandwidth of excitation frequencies. This limitation is imposed by the excitation method using an impact hammer. Although the impact hammer is well controlled, it has difficulties for properly exciting very high frequencies as needed in high speed rotating machines. A non contacting (magnetic) excitation system would be perhaps more appropriate.

The identified dynamic coefficients show the expected trends with increasing rotation speed but the non zero value of the cross coupling damping is a indication of the measurement error. The accuracy of the direct and cross coupling stiffness and of the direct damping coefficients is validated by comparisons with unbalance test responses.

Further work will be devoted to the consolidation of measurements and to comparisons with theoretical predictions. At long term the test rig will be also adapted for an elastic rotor and for different bearings.

ACKNOWLEDGMENTS

The authors are grateful to *Snecma Space Engine Division* and to *Centre National d'Etudes Spatiales* for supporting this activity.

REFERENCES

[1] Constantinescu, V.N., 1969, *Gas Lubrication*, The American Society of Mechanical Engineering (translated from Romanian, *Lubrificatia cu gaze*, Editura Academiei, 1963)

[2] ***, 1967, *Design of Gas Bearings*, Mechanical Technology Incorporated.

[3] Powell, J.W., 1970, *Design of Aerostatic Bearings*, The Machinery Publishing Co. Ltd.

[4] Gross, W.A., Match, L.A., Castelli, V., Eshel, A., Vohr, J.H., Wildmann, M., 1980, *Fluid Film Lubrication*, Wiley New York.

[5] Diaz, S., Beets, T., Dunn, G., San Andrés, L., 1999, "High Speed Test Rig for Identification of Gas Journal Bearing Performance: Design, Constraints and Fabrication," TRC-RD-1-99.

[6] Wilde, D.A., and San Andrés, L., 2006, "Experimental Response of Simple Gas Hybrid Bearings for Oil-Free Turbomachinery," ASME Journal of Engineering for Gas Turbines and Power, 128, pp. 626-633.

[7] Ryu, K., and L. San Andrés, 2006, "Measurements of Rotordynamic Response of a Rotor Supported on Hybrid Flexure Pivot Tilting Pad Gas Bearings" Paper IJTC 2006-12371, ASME/STLE International Joint Tribology Conference, San Antonio, TX, October 2006

[8] Zhu, S. and L., San Andrés, 2007, "Rotordynamic Performance of Flexure Pivot Hydrostatic Gas Bearings for Oil-Free Turbomachinery," Journal of Engineering for Gas Turbines and Power, 129(4), pp. 1020-1027. (ASME Paper GT 2004-53621)

[9] San Andrés, L., and Ryu, K., 2008, "Hybrid Gas Bearings with Controlled Supply Pressure to Eliminate Rotor Vibrations while Crossing System Critical Speeds," ASME Journal of Engineering for Gas Turbines and Power, Vol. 130(6), pp. 062505-1-10.

[10] Belforte, G., Raparelli, T., Viktorov, V., Trivella, A., Colombo, F., 2006, « An Experimental Study of High Speed Rotors Supported by Air Bearings; Test Rig and First Experimental Results", Tribology International, Vol. 39, pp. 834-845.

[11] Belforte, G., Raparelli, T., Viktorov, V., Trivella, A., Colombo, F., 2006, « Study of A High Speed Electrospindle With Air Bearings", European Conference on Tribology, ECOTRIB 2007, June 12-15, Vol. 2, pp. 969-982, Ljubliana Slovenia.

[12] Colombo, F., Trivella, A., 2008, "Air Bearing Testing", International Journal of Fluid Power, 9, No.3, pp. 45-53.

[13] De Santiago, O.C., 2002, *Identification of Bearing Supports' Force Coefficients From Rotor Responses Due to Imbalances and Impact Loads*, PhD Dissertation Texas A&M University.

[14] Bonneau, O., Frêne, J., Arghir, M., 2008, "A new test rig for measuring the dynamic characteristics of labyrinth seals and hybrid bearings at very high Reynolds numbers" 35th Leeds-Lyon Symposium on Tribology, 9 – 12 September, Leeds, England.

[15] Murphy, B.T., Wagner, M.N., 1991, "Measurement of Rotordynamic Coefficients for a Hydrostatic Radial Bearing", ASME Journal of Tribology, 113(2), pp. 518-252.